The Astrophysical Journal, 790:52 (9pp), 2014 July 20 doi:10.1088/0004-637X/790/1/52

NO X-RAYS FROM THE VERY NEARBY TYPE Ia SN 2014J: CONSTRAINTS ON ITS ENVIRONMENT

R. Margutti[1], J. Parrent[1], A. Kamble[1], A. M. Soderberg[1], R. J. Foley[2,3],
D. Milisavljevic[1], M. R. Drout[1], and R. Kirshner[1]
[1] Harvard-Smithsonian Center for Astrophysics, 60 Garden St., Cambridge, MA 02138, USA
[2] Astronomy Department, University of Illinois at Urbana–Champaign, 1002 W. Green Street, Urbana, IL 61801, USA
[3] Department of Physics, University of Illinois Urbana–Champaign, 1110 W. Green Street, Urbana, IL 61801, USA
Received 2014 May 6; accepted 2014 June 2; published 2014 July 2

ABSTRACT

Deep X-ray observations of the post-explosion environment around the very nearby Type Ia SN 2014J ($d_{\rm L}$ = 3.5 Mpc) reveal no X-ray emission down to a luminosity $L_x < 7 \times 10^{36}$ erg s^{-1} (0.3–10 keV) at $\delta t \sim 20$ days after the explosion. We interpret this limit in the context of inverse Compton emission from upscattered optical photons by the supernova shock and constrain the pre-explosion mass-loss rate of the stellar progenitor system to be $\dot{M} < 10^{-9}\, M_{\odot}$ yr^{-1} (for wind velocity $v_w = 100$ km s^{-1}). Alternatively, the SN shock might be expanding into a uniform medium with density $n_{\rm CSM} < 3$ cm^{-3}. These results rule out single-degenerate (SD) systems with steady mass loss until the terminal explosion and constrain the fraction of transferred material lost at the outer Lagrangian point to be $\leqslant$1%. The allowed progenitors are (1) white dwarf–white dwarf progenitors, (2) SD systems with unstable hydrogen burning experiencing recurrent nova eruptions with recurrence time $t < 300$ yr, and (3) stars where the mass loss ceases before the explosion.

Key word: supernovae: individual (SN 2014J)

Online-only material: color figures

1. INTRODUCTION

Type Ia supernovae (SNe) are believed to originate from white dwarfs (WDs) in binary systems. However, no stellar progenitor has ever been directly identified in pre-explosion images, not even for the two closest Type Ia SNe discovered in the last 25 yr: SN 2011fe (Li et al. 2011) and, more recently, SN 2014J (Kelly et al. 2014; Goobar et al. 2014). As a result, the nature of their progenitor system is still a matter of debate (e.g., Howell 2011; Di Stefano et al. 2013; Maoz et al. 2013). Here we present a detailed study of SN 2014J at X-ray energies, with the primary goal to constrain the circumstellar environment of the exploding star.

SN 2014J was discovered by Fossey et al. (2014) in the nearby starburst galaxy M82. At the distance of $d_{\rm L} = 3.5$ Mpc (Dalcanton et al. 2009; Karachentsev & Kashibadze 2006), SN 2014J is the nearest Type Ia SN discovered in the last three decades and offers an unprecedented opportunity to study the progenitor system of thermonuclear stellar explosions.

Type Ia SNe are believed to originate from the runaway thermonuclear explosion of a degenerate C/O stellar core, likely a WD in a binary system (Hoyle & Fowler 1960; Colgate & McKee 1969; see Calder et al. 2013, Maoz et al. 2013, and Parrent et al. 2014 for recent reviews). While there is consensus that a WD explodes, the astronomical events that precede the explosion are less clear.

Two progenitor channels are mostly favored, involving non-degenerate and degenerate binary companions, respectively. In the first scenario (single degenerate, SD, hereafter), the WD accretes material from the companion, potentially a giant, sub-giant or main-sequence star (Whelan & Iben 1973; Hillebrandt & Niemeyer 2000; Nomoto 1982b). Wind from the secondary star provides material to be accreted (symbiotic channel; see, e.g., Patat et al. 2011). Mass can be transferred to the WD via Roche lobe overflow (RLOF) from a hydrogen-rich mass-donor star or He star (Nomoto 1982a; van den Heuvel et al. 1992; Iben & Tutukov 1994; Yoon & Langer 2003). The second standard scenario involves two WDs (double-degenerate scenario, DD, hereafter; Iben & Tutukov 1984; Webbink 1984). The explosion occurs as the two WDs merge as a consequence of the loss of angular momentum.

The two classes of progenitor systems are predicted to leave different imprints on the circumbinary environment. For SD progenitor channels the local environment is expected to be either directly enriched by wind from the donor star (symbiotic systems) or by non-conservative mass transfer (i.e., by matter that the WD is unable to accrete). For the DD scenario the general expectation is that of a "cleaner" environment with density typical of the interstellar medium (ISM). Particularly intriguing in this respect is the evidence for interaction of the SN ejecta with circumbinary material as revealed by optical observations of some Type Ia SNe (see, e.g., Silverman et al. 2013).

The nearby SN environment can also be revealed by using sensitive X-ray observations obtained shortly after the explosion (e.g., Russell & Immler 2012; Horesh et al. 2012; Margutti et al. 2012). For both the SD and DD scenarios, the X-ray emission is powered by the interaction of the SN shock with the circumburst medium and can thus be used as a probe of the local environment (e.g., Chevalier & Fransson 2006). Here we present the results from deep *Chandra* X-ray observations of SN 2014J that enable us to put stringent constraints on the progenitor system mass loss prior to explosion. X-ray observations are described in Section 2. We re-construct the bolometric light-curve of SN 2014J from broadband optical photometry spanning the UV to near-IR (NIR) range in Section 3. We combine the optical and X-ray observations to derive a deep limit to the mass-loss rate of the progenitor system of SN 2014J in Section 4. The mass-loss limit is used to infer the nature of the donor star in

the progenitor system of SN 2014J in Section 5. Conclusions are drawn in Section 6.

Uncertainties are quoted at a 1σ confidence level, unless otherwise noted. Throughout the paper we use 2014 January 14.72 UT as the explosion date of SN 2014J (Zheng et al. 2014). The possible presence of a "dark phase" (e.g., Piro & Nakar 2013, 2014) with a duration between hours and a few days between the explosion and the time of the first emitted light has no impact on our major conclusions.

2. OBSERVATIONS AND DATA ANALYSIS

2.1. Swift-XRT

The *Swift* (Gehrels et al. 2004) X-Ray Telescope (XRT; Burrows et al. 2005) started observing SN 2014J on 2014 January 22, 10:13:52 UT ($\delta t \sim 8$ days; PI: Brown, PI: Ofek). XRT data have been analyzed using HEASOFT (v6.15) and corresponding calibration files. Standard filtering and screening criteria have been applied. We find no evidence for a point-like X-ray source at the position of SN 2014J. Using observations acquired at $\delta t < 20$ days (total exposure time of 114 ks), the $3\,\sigma$ count-rate limit is 2.4×10^{-3} counts s^{-1} in the 0.3–10 keV energy range. The Galactic neutral hydrogen column density in the direction of SN 2014J is $\mathrm{NH_{MW}} \lesssim 5.1 \times 10^{20}\,\mathrm{cm^{-2}}$ (Kalberla et al. 2005).[4] The estimate of the intrinsic hydrogen column ($\mathrm{NH_{int}}$) is more uncertain. Observations of SN 2014J at optical wavelengths point to a large local extinction (see Section 3) corresponding to $A_V = 1.7 \pm 0.2$ mag (Goobar et al. 2014). A more recent study by Amanullah et al. (2014) find consistent results around maximum light: $A_V = 1.9 \pm 0.1$ mag. Assuming a Galactic dust-to-gas ratio, this would imply $\mathrm{NH_{int}} \sim 4 \times 10^{21}\,\mathrm{cm^{-2}}$ (Predehl & Schmitt 1995; Watson 2011). However, the low value inferred for the total-to-selective extinction $R_V < 2$ (Goobar et al. 2014; Amanullah et al. 2014) suggests the presence of smaller dust grains, more similar to the grain size distribution of the Small Magellanic Cloud (SMC). For an SMC-like dust-to-gas ratio the inferred hydrogen column is $\mathrm{NH_{int}} \sim (7\text{–}15) \times 10^{21}\,\mathrm{cm^{-2}}$ (Martin et al. 1989; Welty et al. 2012). Gamma-ray burst (GRB) host galaxies sample instead the high end of the gas-to-dust ratio distribution (Schady et al. 2010). For a GRB-like environment the observed optical extinction would imply $\mathrm{NH_{int}} \sim 10^{22}\,\mathrm{cm^{-2}}$. Based on these findings, in the following we calculate our flux limits and results for a fiducial range of intrinsic hydrogen column density values: $4 \times 10^{21}\,\mathrm{cm^{-2}} < \mathrm{NH_{int}} < 10^{22}\,\mathrm{cm^{-2}}$. We adopt $\mathrm{NH_{int}} \sim 7 \times 10^{21}\,\mathrm{cm^{-2}}$ as "central value" in our calculations.[5] It is worth noting that from the analysis of diffuse interstellar bands (DIBs) in M82, Welty et al. (2014) estimate a total hydrogen column density of $\sim 5 \times 10^{21}\,\mathrm{cm^{-2}}$ in the direction of SN 2014J.

Based on these values, the unabsorbed XRT flux limit is $F_x^{3\sigma} < 2.4 \times 10^{-13}\,\mathrm{erg\,s^{-1}cm^{-2}}$ ($\mathrm{NH_{int}} = 7 \times 10^{21}\,\mathrm{cm^{-2}}$), corresponding to $L_x^{3\sigma} < 3.5 \times 10^{38}\,\mathrm{erg\,s^{-1}}$. Restricting our analysis to $7 \lesssim \delta t \lesssim 15$ days, when X-ray inverse Compton (IC) emission is expected to peak (Figure 2), we find a count-rate limit of $5.4 \times 10^{-3}\,\mathrm{c\,s^{-1}}$ (exposure time of 27 ks, 0.3–10 keV), corresponding to $F_x^{3\sigma} < 5.5 \times 10^{-13}\,\mathrm{erg\,s^{-1}cm^{-2}}$ with $L_x^{3\sigma} < 8.0 \times 10^{38}\,\mathrm{erg\,s^{-1}}$.

2.2. Chandra

We initiated deep X-ray follow up of SN 2014J with the *Chandra X-ray Observatory* on 2014 February 3, 20:10:39 UT ($\delta t \sim 20.4$ days) under an approved Director's Discretionary Time proposal (PI: Margutti). Data have been reduced with the CIAO software package (version 4.6) and corresponding calibration files. Standard ACIS data filtering has been applied. The total exposure time of our observations is 47 ks. The observations mid-time corresponds to $\delta t = 20.4$ days since the explosion. No X-ray source is detected at the SN position (Figure 1) with a 3σ upper limit of 2.1×10^{-4} counts s^{-1} in the 0.3–10 keV energy band, which implies an absorbed flux limit of $F_x < 2.6 \times 10^{-15}\,(\mathrm{erg\,s^{-1}cm^{-2}})$ for an assumed $F_\nu \propto \nu^{-1}$ spectrum. The count-rate limit is calculated as a 3σ fluctuation from the local background assuming Poisson statistics as appropriate in the regime of low-count statistics. The presence of diffuse soft X-ray emission from the host galaxy (Figure 1, left panel) prevents us from reaching deeper limits.

The unabsorbed flux limit is $F_x^{3\sigma} < 5.0 \times 10^{-15}\,\mathrm{erg\,s^{-1}cm^{-2}}$ ($\mathrm{NH_{int}} = 7 \times 10^{21}\,\mathrm{cm^{-2}}$, 0.3–10 keV energy band), with $(4.0 < F_x^{3\sigma} < 6.0) \times 10^{-15}\,\mathrm{erg\,s^{-1}cm^{-2}}$ for the range of $\mathrm{NH_{int}}$ values above. At the distance of 3.5 Mpc, the corresponding luminosity limit is $L_x^{3\sigma} < 7.2 \times 10^{36}\,\mathrm{erg\,s^{-1}}$, with $(5.7 < L_x^{3\sigma} < 8.7) \times 10^{36}\,\mathrm{erg\,s^{-1}}$.

3. THE BOLOMETRIC LUMINOSITY OF SN 2014J

The line of sight toward SN 2014J is heavily reddened by dust in the host galaxy. The Galactic reddening in the direction of the SN is $E(B-V)_{\mathrm{MW}} = 0.06$ mag (Dalcanton et al. 2009). The analysis of the spectra and broadband photometry of SN 2014J by Goobar et al. (2014) indicates a local color excess $E(B-V)_{\mathrm{host}} \sim 1.2$ mag and a low value of total-to-selective extinction $R_V < 2$. These results are consistent with earlier reports by Cox et al. (2014) and Patat et al. (2014). In the remaining of the paper we follow Goobar et al. (2014) and use $E(B-V)_{\mathrm{host}} = 1.22 \pm 0.05$ mag with $R_V^{\mathrm{host}} = 1.40 \pm 0.15$ mag.[6] The uncertainty on the local extinction parameters is consistently propagated into our final bolometric luminosity (Figure 2, lower panel).

To derive the bolometric luminosity of SN 2014J we start from the *UBVRYJHK* and *iz* photometry published by Goobar et al. (2014). We complement this photometric data set with additional *JHK* photometry from Venkataraman et al. (2014), Srivastav et al. (2014), and Richardson et al. (2014) and obtain extinction corrected flux densities applying a Cardelli et al. (1989) extinction law with the color excess and the total-to-selective extinction values as above (in addition to the Galactic correction). A first, pseudo-bolometric light curve of SN 2014J is then obtained by integrating the extinction corrected flux

[4] A careful analysis of the 21 cm radio emission suggests that this value might be contaminated by gas in M82 and that the actual contribution from the Galaxy might be closer to $3.7 \times 10^{20}\,\mathrm{cm^{-2}}$ (Welty et al. 2014). We note that the use of this lower $\mathrm{NH_{MW}}$ value would have no impact on our conclusions.

[5] Based on pre-explosion *Chandra* observations, Nielsen et al. (2014) infer $\mathrm{NH_{int}} = (8.6 \pm 0.4) \times 10^{21}\,\mathrm{cm^{-2}}$. However, the actual X-ray absorption affecting SN 2014J can be either smaller or larger, depending if SN 2014J exploded in front of some of the material responsible for the intrinsic hydrogen column in pre-explosion images or if instead SN 2014J illuminated additional material which was not contributing to the measured $\mathrm{NH_{int}}$.

[6] The properties of DIBs in the spectra of SN 2014J would indicate a higher local extinction corresponding to $A_V^{\mathrm{host}} = 2.5 \pm 0.1$ mag (Goobar et al. 2014, see, however, Welty et al. 2014 who find $A_V^{\mathrm{host}} = 1.6$–$2.1$ mag). A later study by Amanullah et al. (2014) finds $A_V^{\mathrm{host}} = 1.9 \pm 0.1$ mag. The parameters adopted above imply instead $A_V^{\mathrm{host}} = 1.7 \pm 0.2$ mag which leads to more conservative limits to the mass-loss rate of the progenitor system derived in Section 4.

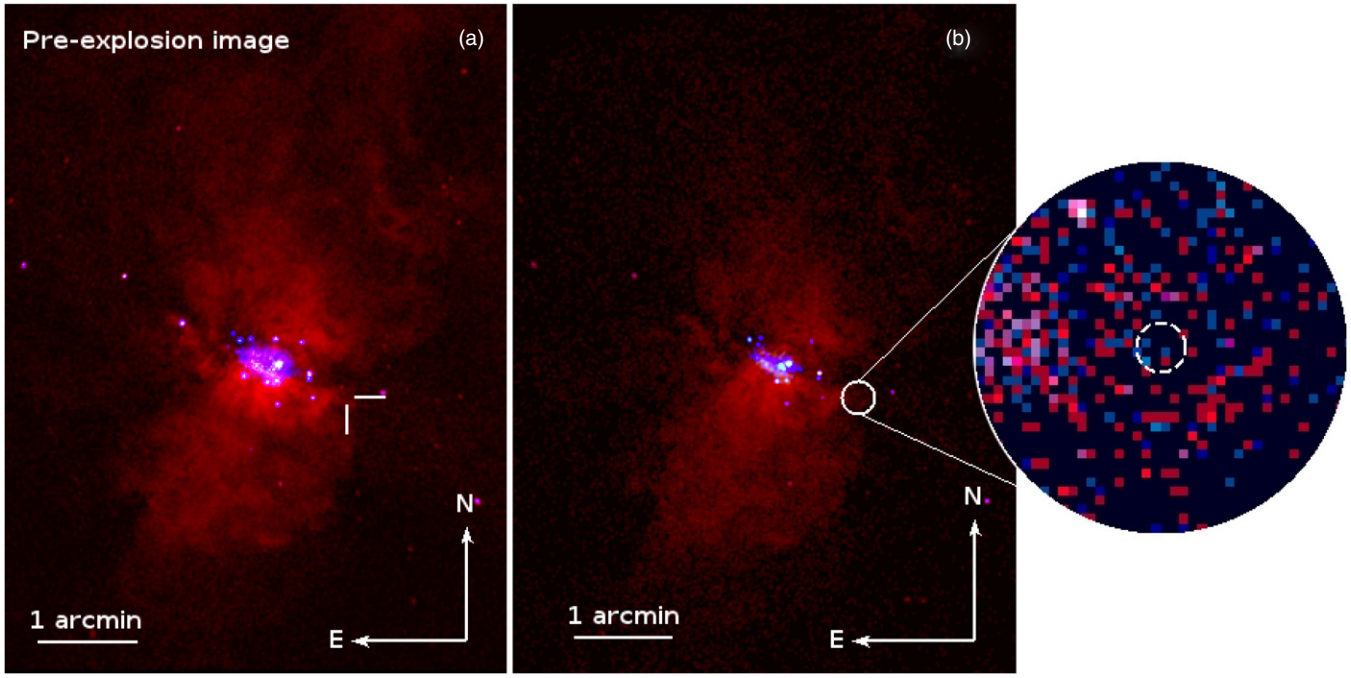

Figure 1. False-color pre-explosion (left panel) and post-explosion (central panel) images of the environment around the Type Ia SN 2014J obtained with the *Chandra X-ray Observatory*. Right panel: zoom-in to the SN location. The dashed circle has a radius of 0.″9 around the position of SN 2014J (*Chandra* PSF at 1.5 keV, 90% containment). No X-ray emission is detected at the position of SN 2014J, enabling deep limits on the mass-loss rate of the stellar progenitor system. The pre-explosion image combines 237 ks of archival *Chandra* data (PI: Strickland). Our post-explosion observations obtained at $\delta t = 20.4$ days are shown in panel (b) (exposure time of 47 ks, PI: Margutti). Red, green, and blue colors refer to soft (0.3–1.4 keV), medium (1.4–3 keV), and hard (3–10 keV) photons, respectively.

(A color version of this figure is available in the online journal.)

densities from the U band ($\lambda \sim 3650$ Å) to the K band ($\lambda \sim 2.2\,\mu$m). From well monitored "normal" Type Ia SNe like SN 2011fe we estimate that the amount of flux redward the K band is $\lesssim$5% at $\delta t \lesssim 20$ days since the explosion.

An UV photometric campaign (PI: Brown) has also been carried out with the *Swift* (Gehrels et al. 2004) UV Optical Telescope (Roming et al. 2005). However, the large local extinction makes any extinction correction to the UV photometry extremely uncertain. For this reason we employ a different approach. We estimate the time-varying amount of flux emitted blueward the U band by SN 2014J using the well-monitored, minimally reddened, normal Type Ia SN 2011fe as template (Brown et al. 2012; Margutti et al. 2012). At the time of the *Chandra* observation ($\delta t = 20.4$ days) the UV flux represents (13 ± 5)% of the bolometric flux.

Figure 2, lower panel, shows the final bolometric light-curve of SN 2014J. The displayed uncertainty is driven by the inaccurate knowledge of the local extinction correction. In this work we use the estimates of $A_V^{\rm host}$ and $R_V^{\rm host}$ that appeared in the literature so far. It is possible that later estimates will somewhat deviate from the numbers assumed here. A detailed analysis has been recently published by Foley et al. (2014). We emphasize that a wrong choice of extinction parameters would have no impact on our conclusions as long as it does not lead to an overestimate of the bolometric luminosity of SN 2014J at ~20 days. The comparison with the *UBVRI* light curves of a sample of Type Ia SNe in Figure 2 suggests that we might have instead *underestimated* the bolometric luminosity of SN 2014J. The study by Amanullah et al. (2014) finds that SN 2014J is indeed similar to SN 2011fe once corrected for the extinction. If this is true, then our limits on the density of the explosion local environment should be considered conservative, thus strengthening our conclusions on the progenitor system of SN 2014J of Section 5. A larger $L_{\rm bol}$ would require a smaller environment density in order to avoid detection of X-rays through IC scattering.

4. CONSTRAINTS ON THE PROGENITOR SYSTEM MASS-LOSS RATE

Deep X-ray observations constrain the density of the explosion circumstellar environment, previously shaped by the mass loss of the progenitor system. For hydrogen-stripped progenitors in low density environments, at $\delta t \lesssim 40$ days, the X-ray emission is dominated by IC scattering of photospheric optical photons by relativistic electrons accelerated by the SN shock (Chevalier & Fransson 2006). Following the generalized formalism developed in Margutti et al. (2012), the IC luminosity directly tracks the SN optical luminosity ($L_{\rm IC} \propto L_{\rm bol}$) and further depends on the density structure of the SN ejecta $\rho_{\rm SN}$, the structure of the circumstellar medium $\rho_{\rm CSM}$ and the details of the electron distribution responsible for the upscattering of the optical photons to X-ray energies. The dynamical evolution of the shockwave is treated self-consistently. Finally, since $L_{\rm IC} \propto L_{\rm bol}$, any uncertainty on the estimate of the SN distance from the observer would equally affect $L_{\rm IC}$ and $L_{\rm bol}$, and thus has no impact on the limits we derive on the environment density.

In the following we assume the SN outer density structure to scale as $\rho_{\rm SN} \propto R^{-n}$ with $n \sim 10$, as found for SNe arising from compact progenitors (e.g., Matzner & McKee 1999). Electrons are assumed to be accelerated in a power-law distribution $n(\gamma) \propto \gamma^{-p}$ with index $p = 3$, as supported by radio observations of SN shocks in Type Ib/c explosions (e.g., Soderberg et al. 2006). The fraction of post-shock energy density in relativistic electrons is $\epsilon_e = 0.1$ (Chevalier & Fransson

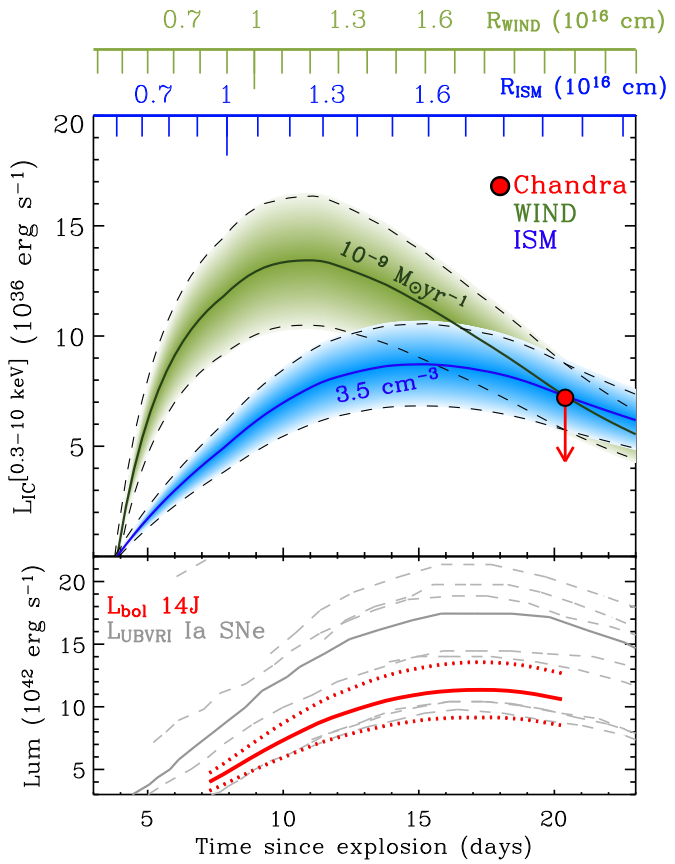

Figure 2. Upper panel: inverse Compton X-ray luminosity expected in the case of wind (green solid line) and ISM (blue solid line) environments. The deep X-ray limit obtained with *Chandra* constrains $\dot{M} < 1.2 \times 10^{-9}\ M_\odot\ \mathrm{yr}^{-1}$ (wind) or $n_{\rm CSM} < 3.5\ \mathrm{cm}^{-3}$ (ISM). The shaded areas mark the range of allowed limits, derived by conservatively accounting for the uncertainty on $L_{\rm bol}$ and $\mathrm{NH_{int}}$: $\dot{M} = (0.7\text{–}2.5) \times 10^{-9}\ M_\odot\ \mathrm{yr}^{-1}$ (wind) and $n_{\rm CSM} = (1.5\text{–}8.0)\ \mathrm{cm}^{-3}$ (ISM). Lower panel: optical bolometric luminosity of SN 2014J (thick line) and associated uncertainty (dotted lines). A sample of *UBVRI* light curves of Type Ia SNe including SNe 1989B, 1991T, 1992A, 1992bc, 1992bo, 1994D, 1994ae, 1995D, 2011fe (thick solid line), 2012cg, is also shown for comparison (from Munari et al. 2013).

(A color version of this figure is available in the online journal.)

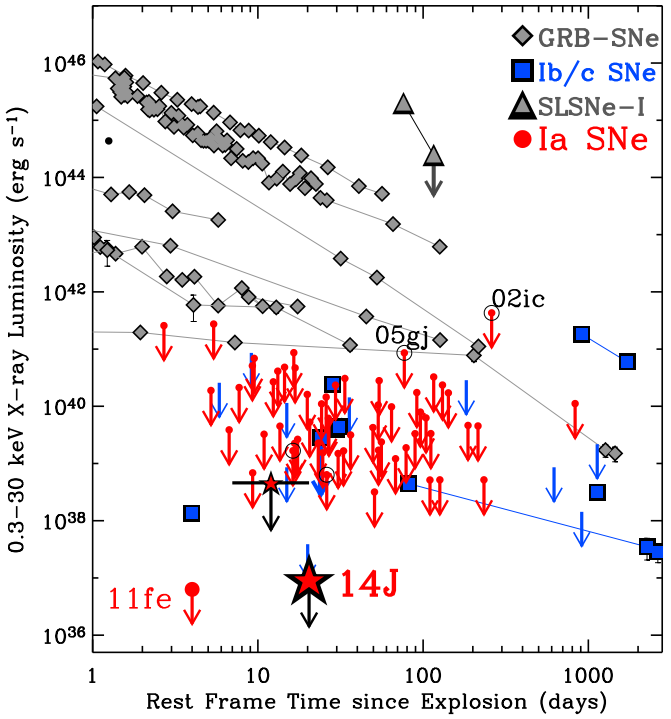

Figure 3. Type I SN explosions in the X-ray phase space, including GRB-SNe (Margutti et al. 2013), ordinary Type Ib/c SNe (Margutti et al. 2014 and references therein), super-luminous hydrogen poor SNe (SLSNe-I; Levan et al. 2013) and Type Ia SNe (Russell & Immler 2012; Schlegel & Petre 1993; Hughes et al. 2007). The emission from SN 2011fe (Margutti et al. 2012) and SN 2014J (big and small star, from *Chandra* and *Swift*-XRT observations, respectively) is much weaker than any hydrogen-poor core-collapse SN ever detected in the X-rays, and represent the deepest limit on the X-ray emission of a Type I SN to date. Open black symbols mark Type Ia SNe with signs of CSM interaction in our sample (i.e., SNe 2002ic, 2005gj, 2006X, 2009ig).

(A color version of this figure is available in the online journal.)

2006). The environment density limits calculated below scale as $(\epsilon_e/0.1)^{-2}$ (Margutti et al. 2012, their Appendix A).

We use the bolometric luminosity light curve derived in Section 3 to constrain the density of the environment around SN 2014J in the case of (1) a wind-like CSM ($\rho_{\rm CSM} \propto R^{-2}$) and (2) an ISM-like CSM ($\rho_{\rm CSM} = \mathrm{const}$). A star which has been losing material at constant rate $\dot{M}$ gives rise to a wind-like CSM. A "wind medium" is the simplest expectation in the case of SD progenitor models. DD progenitor systems would be instead consistent with a "cleaner environment," and, potentially, with an ISM-like CSM. The final result is shown in Figure 2, upper panel.

For a wind-like medium, $\rho_{\rm CSM} = \dot{M}/(4\pi R^2 v_w)$, where $\dot{M}$ is the progenitor pre-explosion mass-loss rate and v_w is the wind velocity. The X-ray non-detection by *Chandra* at $\delta t = 20.4$ days constrains the progenitor mass-loss rate $\dot{M} < 1.2 \times 10^{-9}\ M_\odot\ \mathrm{yr}^{-1}$ for $v_w = 100\ \mathrm{km\ s}^{-1}$. This limit is obtained by using our fiducial $L_{\rm bol}$ (thick line in Figure 2, lower panel) and $L_x^{3\sigma} < 7.2 \times 10^{36}\ \mathrm{erg\ s}^{-1}$ (Section 2.2). Conservatively accounting for the uncertainties affecting our estimates of the bolometric optical luminosity and intrinsic neutral hydrogen absorption column, the range of allowed limits to the progenitor mass-loss rate is (0.7–2.5) $\times 10^{-9}\ M_\odot\ \mathrm{yr}^{-1}$ (shaded areas in Figure 2, upper panel). In a wind-like scenario $\dot{M}/v_w \propto (1/L_{\rm bol})^{1/0.64}$. For an ISM-like medium we find $n_{\rm CSM} < 3.5\ \mathrm{cm}^{-3}$. The range of allowed limits is $(1.5\text{–}8.0)\ \mathrm{cm}^{-3}$ and the particle density scales as $(1/L_{\rm bol})^{0.5}$.

Swift-XRT observations have been acquired starting from $\delta t = 8$ days and cover the time interval when IC X-ray emission peaks. From Figure 2, $L_{\rm IC}^{\rm peak} < 2 \times 10^{37}\ \mathrm{erg\ s}^{-1}$, consistent with the X-ray limit derived from XRT observations $L_x^{3\sigma} < 8.0 \times 10^{38}\ \mathrm{erg\ s}^{-1}$ (Section 2.1).

5. DISCUSSION

Deep X-ray observations obtained around optical maximum light of the nearby SN 2014J allowed us to obtain the most constraining limits on the environment density around a Type Ia SN explosion. With SN 2011fe (Margutti et al. 2012) and SN 2014J (this work), we have probed X-ray luminosities which are a factor ~100 deeper than previously obtained limits (Figure 3), thus sampling a new territory in the X-ray luminosity versus time phase space. However, no X-ray emission is detected in either case, in sharp contrast with hydrogen-stripped core-collapse explosions (squares, diamonds, and triangles in Figure 3).

These observations directly constraint the density of material in the SN immediate environment, shaped by the progenitor system before the terminal explosion. Irrespective of the assumed circumburst density profile, the deep X-ray limit

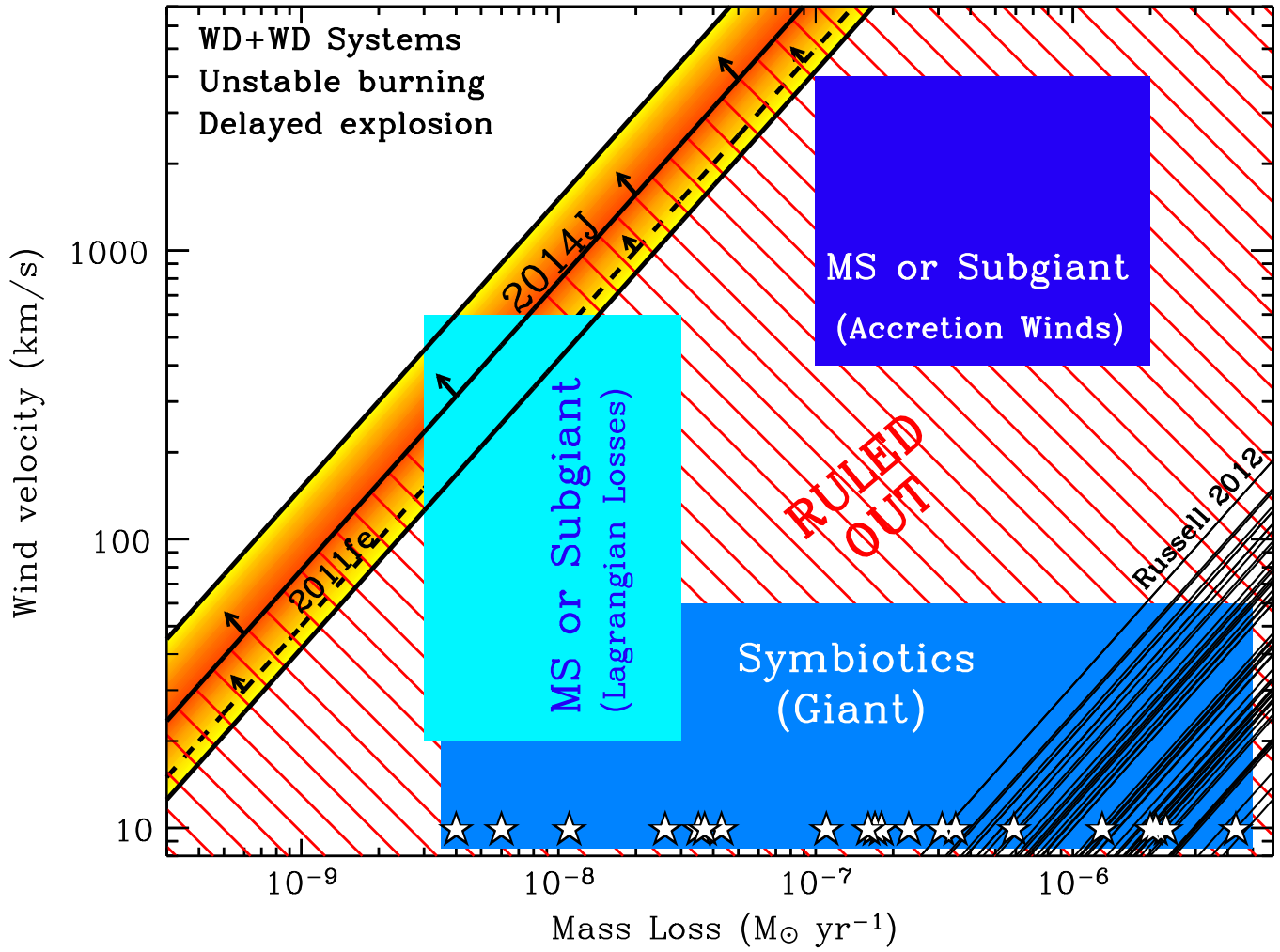

Figure 4. Wind velocity vs. mass-loss phase space. The deep limits we obtain for SN 2014J (colored area) rule out most of the parameter phase space associated with SD models with steady mass loss to the environment. The limit obtained from the X-ray observations of SN 2011fe (dashed line, from Margutti et al. 2012) and the set of limits obtained by Russell & Immler (2012) on a sample of Type Ia SNe (solid black lines) are also shown for comparison. White stars: measured mass loss of symbiotic systems in our Galaxy for an assumed $v_w = 10\,\mathrm{km\,s^{-1}}$ (Seaquist & Taylor 1990).

(A color version of this figure is available in the online journal.)

implies a "clean" environment at distances $R \lesssim 10^{16}$ cm from the explosion center of SN 2014J. We interpret this finding in the context of different progenitor configurations, both for SD and DD models.

5.1. SD with Quasi-steady Mass Loss

WDs around the Chandrasekhar mass $M_{\rm Ch}$ accreting at a rate $M_{\rm acc} \gtrsim 3 \times 10^{-7}\,M_\odot\,\mathrm{yr^{-1}}$ undergo steady hydrogen burning (e.g., Iben 1982; Nomoto 1982b; Prialnik & Kovetz 1995; Shen & Bildsten 2007). In this regime the WD accretes and retains matter. However, the system also loses material to the environment in three different ways: (1) wind from the donor star, (2) non-conservative mass transfer through RLOF, and (3) optically thick winds from the WD.

In symbiotic systems the wind from the giant companion star dominates the mass loss, with typical rates $\dot{M} = 5 \times 10^{-9}$ to $5 \times 10^{-6}\,M_\odot\,\mathrm{yr^{-1}}$ and wind velocities $v_w < 100\,\mathrm{km\,s^{-1}}$ (Seaquist & Taylor 1990; Patat et al. 2011; Chen et al. 2011). Our limit on the environment density around SN 2014J strongly argues against this progenitor scenario (Figure 4). From the analysis of the complete set of pre-explosion images (near UV to NIR) at the SN site acquired with the *Hubble Space Telescope*, Kelly et al. (2014) exclude SD progenitor systems with a bright red giant donor star. Consistent with these results, the mass-loss limit we derived from deep X-ray observations of the SN environment firmly and independently rules out this possibility and extends the conclusion to the entire class of red giant secondary stars.

For systems harboring a main sequence, subgiant or helium star, the dominant source of mass loss to the surroundings is through non conservative mass transfer from the donor to the primary, accreting star. In this scenario the secondary star fills its Roche lobe and some of the transferred material is lost to the environment at the outer Lagrangian point: $\dot{M}_{\rm trans} = \dot{M}_{\rm acc} + \dot{M}_{\rm lost}$. We use the orbital velocity $v \sim$ a few $100\,\mathrm{km\,s^{-1}}$ (or lower) as typical velocity of the ejected material. Observations of WDs in this regime indicate velocities up to $\sim$600 $\mathrm{km\,s^{-1}}$ which we use in Figure 4 (e.g., Deufel et al. 1999). The efficiency of the accretion process ($\dot{M}_{\rm acc}/\dot{M}_{\rm trans}$) is poorly constrained. Our X-ray limit implies a very high efficiency of $\gtrsim$99% (light-blue region in Figure 4) to avoid detectable signs of interaction with the lost material. A similar value was found for SN 2011fe using deep X-ray and radio observations (Margutti et al. 2012; Chomiuk et al. 2012). In this context Panagia et al. (2006) put

a less constraining limit of >60%–80% on the efficiency of the same process using radio observations of a larger sample of 27 SNe Ia.

At high mass transfer rates, optically thick winds developing at the WD surface are expected to self-regulate the mass accretion to a critical value $\dot{M}_{\rm acc} \sim 7 \times 10^{-7}\,M_{\odot}\,{\rm yr}^{-1}$, the exact value depending on the hydrogen mass fraction and WD mass (Hachisu et al. 1999; Han & Podsiadlowski 2004; Shen & Bildsten 2007). Our analysis argues against this progenitor scenario, even in the case of fast outflows with $v_{\rm w} \sim$ a few 1000 km s^{-1} (dark blue region in Figure 4).

Finally, thermonuclear burning of hydrogen rich material on the surface of a WD is expected to generate super-soft X-ray emission, which should be thus detectable in pre-explosion images at the SN site. Consistent with our findings above, Nielsen et al. (2014) found no evidence for a super-soft X-ray source at the position of SN 2014J using deep *Chandra* X-ray observations spanning the time range $1 \lesssim t \lesssim 14$ yr before explosion. These observations allowed Nielsen et al. (2014) to rule out SD systems with high effective temperature of the super-soft emission $kT_{\rm eff} > 80$ eV.

5.2. SD with Non-steady Mass Loss

Non-steady mass enrichment of the progenitor surroundings in the years preceding the SN can create a low-density cavity around the explosion, which would naturally explain our X-ray null detection. The evacuated region around the progenitor system can either be (1) the consequence of the cessation of mass loss from the companion star or (2) the result of repeated nova shell ejections by the WD.

Recurrent novae. A WD near the Chandrasekhar mass ($M \geqslant 1.3\,M_{\odot}$) accreting at $\dot{M}_{\rm acc} \sim$ (0.1–3) $\times 10^{-7}\,M_{\odot}\,{\rm yr}^{-1}$ experiences repeated nova explosions as a result of unsteady hydrogen burning on its surface (e.g., Iben 1982; Starrfield et al. 1985; Livio & Truran 1992; Yaron et al. 2005). Shell ejections associated with the nova outbursts evacuate a region around the progenitor system by sweeping up the wind from the companion star. The result is a complex CSM structure, shaped by the fast nova shells and by the slower wind from the donor star. This scenario has been invoked to explain the evidence for interaction in the spectra of some Type Ia SNe (e.g., SN 2002ic; Wood-Vasey & Sokoloski 2006). The main outcome of this process is the presence of regions with very low density, reaching $n_{\rm CSM} \sim 10^{-3}$–1 cm^{-3}, in the proximity of the explosion center even in the case of very powerful winds from the donor star (Figure 5).

The immediate SN environment critically depends on the time of the SN explosion with respect to the time of the last nova shell ejection, as illustrated by Figure 5. Figure 5 shows the results from the simulations by Dimitriadis et al. (2014) for a symbiotic progenitor system consisting of a WD plus red giant star losing material with rate $\dot{M} = 10^{-6}\,M_{\odot}\,{\rm yr}^{-1}$ and wind velocity $v_w = 10$ km s^{-1}. The nova recurrence timescale in this simulations is $\Delta t = 100$ yr.

From Figure 5 it is clear that our observations obtained at $\delta t \sim 20$ days do not probe the range of densities associated with nova cavities.[7] However, *if* the progenitor of SN 2014J experienced recurrent nova outbursts, our X-ray null detection

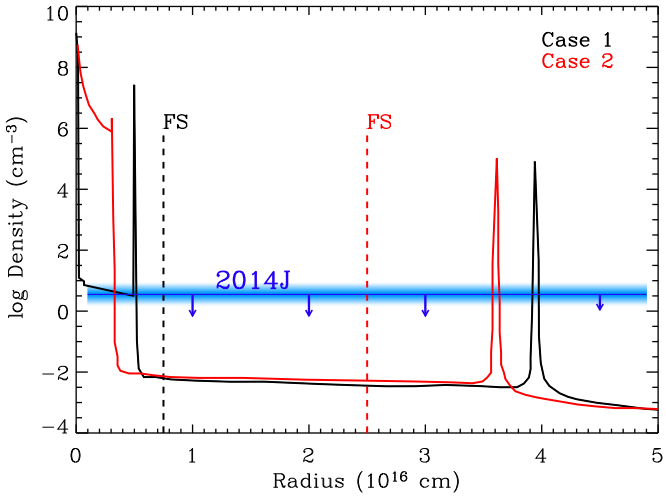

Figure 5. CSM density structure around a symbiotic progenitor system (WD plus red giant star) undergoing repeated nova explosions with a recurrence time $\Delta t = 100$ yr (from Dimitriadis et al. 2014). Case 1: the SN occurs just after the last nova explosion. Case 2: the SN explodes 100 yr after the last nova shell ejection and the nova cavity has been partially refilled by the wind of the red giant star with $\dot{M} = 10^{-6}\,M_{\odot}\,{\rm yr}^{-1}$ and $v_w = 10$ km s^{-1}. Dashed vertical lines: radius of the SN forward shock ∼20 days after the explosion (time of our *Chandra* observations). The CSM densities of the environment sampled by the SN shock at this time are a factor ∼100 smaller than our limit.

(A color version of this figure is available in the online journal.)

implies that (1) a nova shell must have been able to clear out the environment at $R \sim 10^{16}$ cm and (2) the wind from the donor star has not yet been able to refill this volume by the time of the SN explosion.

The size of the cavity cleared out by a nova shell depends on the shell dynamics (e.g., Moore & Bildsten 2012). For typical shell ejection velocities $v_{\rm sh} =$ 1000–4000 km s^{-1} and mass $M_{\rm sh} = 10^{-7}$–$10^{-5}\,M_{\odot}$ (Yaron et al. 2005) expanding into a medium enriched by the secondary star mass loss with a rate $\dot{M} = 10^{-7}$–$10^{-6}\,M_{\odot}\,{\rm yr}^{-1}$, the shell rapidly evolves from free expansion to the Sedov–Taylor phase on a timescale of $t_{\rm ST} \sim$ a few days. It then transitions to the snowplow phase at $t_{\rm SP} \sim$ a few months. Adopting $v_{\rm sh} = 4000$ km s^{-1}, $t_{\rm ST} = 2$ days, $t_{\rm SP} = 2$ months as typical parameters as indicated by observations of the recurrent nova RS Oph (e.g., Bode & Kopal 1987; Mason et al. 1987; Sokoloski et al. 2006), a nova shell would reach $R \sim 10^{16}$ cm on a timescale of ∼40 yr. For a wind environment $R \propto t^{2/3}$ during the Sedov–Taylor phase and $R \propto t^{1/2}$ during the snowplow phase. The slower wind from the donor star would need $\Delta t_{\rm refill} \sim 300$ yr to refill this region with new material (for $v_w = 10$ km s^{-1}).

These results indicate that *if* the recurrent nova scenario applies to SN 2014J, then (1) at least one nova shell has been ejected at $t \geqslant 40$ yr before the SN and (2) the recurrence timescale of nova outbursts is shorter than 300 yr (consistent with the timescales observed in recurrent novae, the shortest known time between outbursts being ∼1 yr at the time of writing; Tang et al. 2014). In this respect it is worth mentioning that a complementary search for nova outbursts in archival optical images revealed no evidence for nova explosions at the location of SN 2014J in the ∼1500 days before the SN (Goobar et al. 2014). No evidence for interaction has been found for SN 2014J at $\delta t \leqslant 20$ days since the explosion, either in the form of light-curve re-brightenings, Hα emission, or time–variable Na D features (Goobar et al. 2014; Zheng et al. 2014; Tsvetkov et al. 2014), consistent with the expansion in a very clean

[7] However, according to Dimitriadis et al. (2014), their Figure 12, we should have been able to detect X-ray emission at the level of $L_x \geqslant 5 \times 10^{37}$ erg s^{-1} at $\delta t \sim 20$ days if the X-rays are of thermal origin. Such emission is clearly ruled out by our observations.

environment. The same conclusion is supported by the deep limits on the radio synchrotron emission by Chomiuk et al. (2014) and Chandler & Marvil (2014).

Cessation of mass loss. Our observations at $\delta t \sim 20$ days cannot exclude the presence of material in the environment at larger distances $R \gtrsim 10^{16}$ cm and are thus consistent with any scenario that predicts cessation of mass loss from the progenitor system at $t \geqslant 300 \times (v_{\rm w}/10\,{\rm km\,s^{-1}})^{-1}$ yr before the terminal explosion ("delayed explosion models" in Figure 4). This condition is naturally satisfied by (1) spin-up/spin-down models (Di Stefano et al. 2011; Justham 2011) and (2) core-degenerate (CD) scenarios for Type Ia SNe (where the WD merges with the core of an asymptotic giant branch, AGB, star; Ilkov & Soker 2012).

In both cases rapid rotation might stabilize the WD against explosion, allowing the WD to grow above $M_{\rm Ch}$. The actual delay time τ between completion of mass transfer and explosion is uncertain and depends on the physical mechanism that regulates the WD spin-down (i.e., reduced accretion, ceased mass transfer, angular momentum transfer, magnetic breaking, gravitational waves). A wide range of values seems to be allowed by theory ($\tau \lesssim 10^5$ yr to $\tau > 10^9$ yr, e.g., Lindblom et al. 1999; Yoon & Langer 2005; Ilkov & Soker 2012; Hachisu et al. 2012). Here it is worth noting that $\tau \geqslant 10^5$ yr is enough for the circumbinary material to become diffuse and reach ISM-like density values at the explosion site, consistent with our findings. Additionally, for $\tau \gtrsim 10^8$–10^9 yr, even if the donors started the mass loss as giant, sub-giant, or main-sequence stars, by the time of the explosion they have exhausted most of their envelopes, their remaining envelopes have shrunk inside their Roche lobes and/or they are likely to have already evolved into compact objects (e.g., He or C/O WDs) or low-mass stars (e.g., Di Stefano et al. 2011; Justham 2011; Hachisu et al. 2012). All these effects would suppress any prominent signature of the mass-donor companion both before (i.e., in pre-explosion images) and after the explosion (i.e., anything that originates from the interaction of the SN shock with the medium), naturally accounting for our null detections.

5.3. WD–WD Progenitors

In double-degenerate models the merger of two WDs leads to the final explosion. The general expectation is that of a "clean" environment at $R \gtrsim 10^{13}$–10^{14} cm with ISM-like density.[8] No stellar progenitor is expected to be detectable at the distance of SN 2014J in near UV to NIR pre-explosion images. Additionally, since the WDs were unlikely to burn hydrogen just prior to explosion, no X-ray source is expected to be found in pre-explosion images either. Our deep X-ray non-detection is consistent with this scenario, but can hardly be considered a confirmation of this progenitor channel. We also note that our results are consistent with the predictions of the CD scenario, where the actual merger involves a WD and the core of an asymptotic giant branch star, as suggested in the case of SN 2011fe (Soker et al. 2014).

WD–WD mergers are, however, expected to enrich the ISM in a number of ways including (1) tidal tail ejections (Raskin & Kasen 2013), (2) mass outflows during the rapid accretion phase before the merger (Guillochon et al. 2010; Dan et al. 2011), (3) winds emanating from the disk during the viscous evolution (Ji et al. 2013), and (4) shell ejections (Shen et al. 2013; see also Soker et al. 2013). Each of these mechanisms predicts the presence of relevant mass at different distances from the explosion center. Below we discuss the predictions of these scenarios at $R \sim 10^{16}$ cm which is relevant for the *Chandra* null detection of SN 2014J.

Tidal tail ejection. Some 10^{-4}–$10^{-2}\,M_\odot$ of material is expected to be tidally stripped and ejected with a typical velocity $v_{\rm ej} \sim 2000\,{\rm km\,s^{-1}}$ just prior to the WD–WD coalescence (Raskin & Kasen 2013). The resulting structure of the CSM and the distance $R_{\rm ej}$ of the overdensity region created by the mass ejection from the explosion center critically depend on the delay time between the tidal tail ejection and the final explosion $\Delta t_{\rm ej}$. In particular, the ejected material would require $\Delta t_{\rm ej} \sim 10^8$ s to reach the distance of interest $R_{\rm ej} \sim 10^{16}$ cm.[9] Raskin & Kasen (2013) calculate that the tidal tail density at this distance would correspond to an effective mass-loss rate $\dot{M} \sim 10^{-2}$–$10^{-5}\,M_\odot\,{\rm yr^{-1}}$ which is ruled out by our observations. Our results thus argue against WD–WD mergers with delay times of the order of 1–10 yr, but allow for short delay times $\Delta t_{\rm ej} < 10^6$ s (including systems that detonate on the dynamical timescale $\Delta t_{\rm ej} \sim 10^2$–$10^3$ s or on the viscous timescale of the remnant disk $\Delta t_{\rm ej} \sim 10^4$–$10^8$ s). Long lag times $\Delta t_{\rm ej} \gg 10^8$ s are also consistent with our findings since the interacting material would be located at larger distances.

Mass outflows during rapid accretion. Guillochon et al. (2010) and Dan et al. (2011) suggested that a phase of mass transfer and rapid accretion (with accretion rates reaching 10^{-5}–$10^{-3}\,M_\odot\,{\rm s^{-1}}$) might precede the actual WD–WD merger. As for SD systems, mass can be lost at the Lagrangian point, thus shaping the environment that the SN shock will probe later on. According to the simulations by Dan et al. (2011), by the time of the merger the mass of the unbound material is $M_{\rm ej} \sim 10^{-2}$–$10^{-3}\,M_\odot$ and could in principle produce observable signatures as soon as the SN shock and ejecta expand and interact with this material. The dynamics of the ejected material depends on $v_{\rm ej}$, $M_{\rm ej}$, and $n_{\rm ISM}$. The location of the ejected material $R_{\rm ej}$ at the time of the SN explosion critically depends on $\Delta t_{\rm ej}$. Both $\Delta t_{\rm ej}$ and $v_{\rm ej}$ are at the moment poorly constrained. For $v_{\rm ej} \sim$ a few $1000\,{\rm km\,s^{-1}}$ (i.e., comparable to the escape velocity), our deep density limit at $R \sim 10^{16}$ cm implies that the system did not eject substantial material in the 2–3 yr before the SN explosion.

Disk winds. WD–WD mergers that fail to promptly detonate have been recently suggested to produce a rapidly rotating, magnetized WD merger surrounded by a hot thick accretion disk before producing a Type Ia SN (Ji et al. 2013). A fraction of the disk mass is lost through magnetically driven winds. Ji et al. (2013) calculate that for near-equal mass WD, $M_{\rm ej} \sim 10^{-3}\,M_\odot$ is gravitationally unbound and ejected with $v_{\rm ej} \sim 2600\,{\rm km\,s^{-1}}$. As for the other scenarios, a critical parameter is the interval of time between the mass ejection and the SN explosion $\Delta t_{\rm ej}$ (assuming that a SN occurs). The low density of SN 2014J at $R \sim 10^{16}$ cm suggests $\Delta t_{\rm ej} >$ a few yr.

Shell ejection. In the case of He + C/O WD progenitors in the context of the "double detonation" model (Livne 1990), Shen et al. (2013) have recently proposed that hydrogen-rich material can be ejected by the binary system in multiple ejection episodes hundreds to thousands of years prior to the merger (see their Figure 3). In their simulations Shen et al. (2013)

[8] Recent DD studies pointed out the possible presence of a region of enhanced density located at $R \sim 10^{13}$–10^{14} cm (e.g., Fryer et al. 2010; Shen et al. 2012; Raskin & Kasen 2013). Its physical origin has to be connected either to the WD–WD merger and/or to the outcome of the subsequent evolution of the system.

[9] Note that for typical ISM densities $n_{\rm ISM} \sim 1\,{\rm cm^{-3}}$, the ejected material is in free expansion for ~200 yr before entering the Sedov–Taylor phase.

find that a total of $M_{\rm ej} = (3\text{–}6) \times 10^{-5}\,M_{\odot}$ of material can be transferred to the environment and it is ejected with initial velocity $v_{\rm ej} \sim 1500\,{\rm km\,s^{-1}}$ (i.e., comparable with the He WD circular velocity). In close analogy to nova shells, the ejected material interacts with the local ISM and shapes the local environment of the explosion (Shen et al. 2013, their Figure 4). Both the delay time between the onset of the mass-transfer and the disruption of the He WD and the time of the last ejection critically depend on the evolutionary history of the He WD, with the "older" He WD in the simulations of Shen et al. (2013) giving origin to mass ejections ∼200 yr before the terminal explosion. Our finding of a very low density environment at $R \sim 10^{16}$ cm constrains the most recent mass ejection in SN 2014J (if any) to have happened at $t > 3$ yr before the explosion.

6. CONCLUSIONS

Type Ia SNe remain among the class of SNe that still lacks both an X-ray and radio counterpart identification. Our *Chandra* monitoring campaigns of the two most nearby SNe Ia in the last 30 yr, SN 2011fe (Margutti et al. 2012) and SN 2014J (this work), allowed us to sample a new region of the L_x versus time parameter space ($L_x < 7 \times 10^{36}\,{\rm erg\,s^{-1}}$; Figure 3), and offered us the opportunity to probe the environment density down to the unprecedented level of a few particles per cm^3 at $R \lesssim 10^{16}$ cm.

Our major findings can be summarized as follows.

1. The deep X-ray null detection of SN 2014J at ∼20 days ($L_x < 7 \times 10^{36}\,{\rm erg\,s^{-1}}$) implies a low-density environment with $n_{\rm CSM} < 3\,{\rm cm^{-3}}$ at $R \sim 10^{16}$ cm from the center of the explosion (ISM medium). For a wind-like density profile, the luminosity above translates into a pre-explosion mass-loss rate $\dot{M} < 10^{-9}\,M_{\odot}\,{\rm yr^{-1}}$ for wind velocity $v_{\rm w} = 100\,{\rm km\,s^{-1}}$. By contrast to limits derived from radio synchrotron emission, our results are independent of assumptions about the poorly constrained post-shock energy density in magnetic fields (e.g., Chomiuk et al. 2012; Horesh et al. 2012 for SN 2011fe).
2. These results rule out with high confidence the majority of the parameter space populated by SD models with steady mass loss until the terminal explosion (Figure 4), and in particular symbiotic systems with a giant companion.
3. *If* the progenitor system of SN 2014J is SD and harbors a main sequence or subgiant mass-donor star undergoing RLOF, our results imply a high efficiency of the accretion process onto the WD $\dot{M}_{\rm acc}/\dot{M}_{\rm trans} \gtrsim 99\%$.
4. In the allowed portion of the progenitor parameter space (Figure 4) we find WD–WD scenarios (both DD with a pair of C/O WDs and He + C/O WDs of the double detonation model), SD systems undergoing unstable hydrogen burning, and SD or DD models where the terminal explosion is delayed with respect to the completion of the mass loss. A delay time as short as $\sim 300 \times (v/10\,{\rm km\,s^{-1}})^{-1}$ yr would be enough to explain our X-ray null detection. Alternatively, SD progenitors burning hydrogen unsteadily experience repeated nova shell ejections. *If* SN 2014J originates from this class of progenitors, our results suggest that, for typical nova-shell and SN environment parameters, (1) at least one nova shell has been ejected at $t \geqslant 40$ yr before the SN, (2) the recurrence time of shell ejection by our system is <300 yr.

This discussion emphasizes that a single deep X-ray observation of a nearby Type Ia SN has strong discriminating power in the case of progenitors with steady mass loss until the terminal explosion. However, a change in the observation strategy, with multiple deep observations obtained in the first ∼100 days since the explosion, is needed to better constrain scenarios with sporadic mass-loss episodes just before the terminal explosion. We advocate for such observations to be obtained for the next Type Ia SN discovered in the local universe ($d < 10$ Mpc). Late-time ($t \gg 100$ days) deep X-ray observations will be able to sample the more distant environment: for example, recent analysis of the Type Ia SN remnant Kepler suggests that CSM cavities may reach out to $R \sim 10^{17}$ cm (Patnaude et al. 2012). This effort must be paralleled by realistic theoretical predictions of the environment density structure around the explosion, possibly shaped by repeated mass ejections from the progenitor system for a wide range of progenitor/environment parameters.

We thank the referee for useful comments and a timely report. We thank H. Tananbaum and the entire *Chandra* team for making the X-ray observations possible. R.M. thanks Lorenzo Sironi, Cristiano Guidorzi, and James Guillochon for many instructive discussions and Georgios Dimitriadis for clarifications about his nova ejection simulations. Support for this work was provided by the David and Lucile Packard Foundation Fellowship for Science and Engineering awarded to A.M.S. R.K. acknowledges support from the National Science Foundation through grant AST12-11196.

REFERENCES

Amanullah, R., Goobar, A., Johansson, J., et al. 2014, ApJ, 788, 21
Bode, M. F., & Kopal, Z. 1987, Ap&SS, 134, 419
Brown, P. J., Dawson, K. S., de Pasquale, M., et al. 2012, ApJ, 753, 22
Burrows, D. N., Hill, J. E., Nousek, J. A., et al. 2005, SSRv, 120, 165
Calder, A. C., Krueger, B. K., Jackson, A. P., & Townsley, D. M. 2013, FrPhy, 8, 168
Cardelli, J. A., Clayton, G. C., & Mathis, J. S. 1989, ApJ, 345, 245
Chandler, C. J., & Marvil, J. 2014, ATel, 5812, 1
Chen, X., Han, Z., & Tout, C. A. 2011, ApJL, 735, L31
Chevalier, R. A., & Fransson, C. 2006, ApJ, 651, 381
Chomiuk, L., Soderberg, A. M., Moe, M., et al. 2012, ApJ, 750, 164
Chomiuk, L., Zauderer, B. A., Margutti, R., & Soderberg, A. 2014, ATel, 5800, 1
Colgate, S. A., & McKee, C. 1969, ApJ, 157, 623
Cox, N. L. J., Davis, P., Patat, F., & Van Winckel, H. 2014, ATel, 5797, 1
Dalcanton, J. J., Williams, B. F., Seth, A. C., et al. 2009, ApJS, 183, 67
Dan, M., Rosswog, S., Guillochon, J., & Ramirez-Ruiz, E. 2011, ApJ, 737, 89
Deufel, B., Barwig, H., Šimić, D., Wolf, S., & Drory, N. 1999, A&A, 343, 455
Di Stefano, R., Orio, M., & Moe, M. (ed.) 2013, in IAU Symp. 281, Binary Paths to Type Ia Supernovae Explosions (Cambridge: Cambridge Univ. Press)
Di Stefano, R., Voss, R., & Claeys, J. S. W. 2011, ApJL, 738, L1
Dimitriadis, G., Chiotellis, A., & Vink, J. 2014, arXiv:1401.7332
Foley, R. J., Fox, O., McCully, C., et al. 2014, arXiv:1405.3677
Fossey, J., Cooke, B., Pollack, G., Wilde, M., & Wright, T. 2014, CBET, 3792, 1
Fryer, C. L., Ruiter, A. J., Belczynski, K., et al. 2010, ApJ, 725, 296
Gehrels, N., Chincarini, G., Giommi, P., et al. 2004, ApJ, 611, 1005
Goobar, A., Johansson, J., Amanullah, R., et al. 2014, ApJ, 784, 12
Guillochon, J., Dan, M., Ramirez-Ruiz, E., & Rosswog, S. 2010, ApJL, 709, L64
Hachisu, I., Kato, M., & Nomoto, K. 1999, ApJ, 522, 487
Hachisu, I., Kato, M., & Nomoto, K. 2012, ApJL, 756, L4
Han, Z., & Podsiadlowski, P. 2004, MNRAS, 350, 1301
Hillebrandt, W., & Niemeyer, J. C. 2000, ARA&A, 38, 191
Horesh, A., Kulkarni, S. R., Fox, D. B., et al. 2012, ApJ, 746, 21
Howell, D. A. 2011, NatCo, 2
Hoyle, F., & Fowler, W. A. 1960, ApJ, 132, 565
Hughes, J. P., Chugai, N., Chevalier, R., Lundqvist, P., & Schlegel, E. 2007, ApJ, 670, 1260
Iben, I., Jr. 1982, ApJ, 259, 244
Iben, I., Jr., & Tutukov, A. V. 1984, ApJS, 54, 335

Iben, I., Jr., & Tutukov, A. V. 1994, ApJ, 431, 264
Ilkov, M., & Soker, N. 2012, MNRAS, 419, 1695
Ji, S., Fisher, R. T., García-Berro, E., et al. 2013, ApJ, 773, 136
Justham, S. 2011, ApJL, 730, L34
Kalberla, P. M. W., Burton, W. B., Hartmann, D., et al. 2005, A&A, 440, 775
Karachentsev, I. D., & Kashibadze, O. G. 2006, Ap, 49, 3
Kelly, P. L., Filippenko, A. V., Modjaz, M., & Kocevski, D. 2014, arXiv:1403.4250
Levan, A. J., Read, A. M., Metzger, B. D., Wheatley, P. J., & Tanvir, N. R. 2013, ApJ, 771, 136
Li, W., Bloom, J. S., Podsiadlowski, P., et al. 2011, Natur, 480, 348
Lindblom, L., Mendell, G., & Owen, B. J. 1999, PhRvD, 60, 064006
Livio, M., & Truran, J. W. 1992, ApJ, 389, 695
Livne, E. 1990, ApJL, 354, L53
Maoz, D., Mannucci, F., & Nelemans, G. 2013, arXiv:1312.0628
Margutti, R., Milisavljevic, D., Soderberg, A. M., et al. 2012, ApJ, 751, 134
Margutti, R., Soderberg, A. M., Chomiuk, L., et al. 2013, MNRAS, 428, 729
Margutti, R., Zaninoni, E., Bernardini, M. G., et al. 2014, arXiv:1402.6344
Martin, N., Maurice, E., & Lequeux, J. 1989, A&A, 215, 219
Mason, K. O., Córdova, F. A., Bode, M. F., & Barr, P. 1987, in RS Ophiuchi (1985) and the Recurrent Nova Phenomenon, ed. M. F. Bode, 167
Matzner, C. D., & McKee, C. F. 1999, ApJ, 510, 379
Moore, K., & Bildsten, L. 2012, ApJ, 761, 182
Munari, U., Henden, A., Belligoli, R., et al. 2013, NewA, 20, 30
Nielsen, M. T. B., Gilfanov, M., Bogdan, A., Woods, T. E., & Nelemans, G. 2014, arXiv:1402.2896
Nomoto, K. 1982a, ApJ, 257, 780
Nomoto, K. 1982b, ApJ, 253, 798
Panagia, N., Van Dyk, S. D., Weiler, K. W., et al. 2006, ApJ, 646, 369
Parrent, J., Friesen, B., & Parthasarathy, M. 2014, Ap&SS, 351, 1
Patat, F., Chugai, N. N., Podsiadlowski, P., et al. 2011, A&A, 530, A63
Patat, F., Taubenberger, S., Baade, D., et al. 2014, ATel, 5830, 1
Patnaude, D. J., Badenes, C., Park, S., & Laming, J. M. 2012, ApJ, 756, 6
Piro, A. L., & Nakar, E. 2014, ApJ, 784, 85
Piro, A. L., & Nakar, E. 2013, ApJ, 769, 67
Predehl, P., & Schmitt, J. H. M. M. 1995, A&A, 293, 889
Prialnik, D., & Kovetz, A. 1995, ApJ, 445, 789
Raskin, C., & Kasen, D. 2013, ApJ, 772, 1
Richardson, N., Artigau, E., Laflamme, D., & Malenfant, B. 2014, ATel, 5840, 1
Roming, P. W. A., Kennedy, T. E., Mason, K. O., et al. 2005, SSRv, 120, 95
Russell, B. R., & Immler, S. 2012, ApJL, 748, L29
Schady, P., Page, M. J., Oates, S. R., et al. 2010, MNRAS, 401, 2773
Schlegel, E. M., & Petre, R. 1993, ApJL, 412, L29
Seaquist, E. R., & Taylor, A. R. 1990, ApJ, 349, 313
Shen, K. J., & Bildsten, L. 2007, ApJ, 660, 1444
Shen, K. J., Bildsten, L., Kasen, D., & Quataert, E. 2012, ApJ, 748, 35
Shen, K. J., Guillochon, J., & Foley, R. J. 2013, ApJL, 770, L35
Silverman, J. M., Nugent, P. E., Gal-Yam, A., et al. 2013, ApJS, 207, 3
Soderberg, A. M., Nakar, E., Berger, E., & Kulkarni, S. R. 2006, ApJ, 638, 930
Soker, N., García-Berro, E., & Althaus, L. G. 2014, MNRAS, 437, L66
Soker, N., Kashi, A., García-Berro, E., Torres, S., & Camacho, J. 2013, MNRAS, 431, 1541
Sokoloski, J. L., Luna, G. J. M., Mukai, K., & Kenyon, S. J. 2006, Natur, 442, 276
Srivastav, S., Ninan, J. P., Anupama, G. C., Sahu, D. K., & Ojha, D. K. 2014, ATel, 5876, 1
Starrfield, S., Sparks, W. M., & Truran, J. W. 1985, ApJ, 291, 136
Tang, S., Bildsten, L., Wolf, W. M., et al. 2014, ApJ, 786, 61
Tsvetkov, D. Y., Metlov, V. G., Shugarov, S. Y., Tarasova, T. N., & Pavlyuk, N. N. 2014, arXiv:1403.7405
van den Heuvel, E. P. J., Bhattacharya, D., Nomoto, K., & Rappaport, S. A. 1992, A&A, 262, 97
Venkataraman, V., Banerjee, D. P. K., Joshi, V., Ashok, N. M., & Bhalerao, V. 2014, ATel, 5793, 1
Watson, D. 2011, A&A, 533, A16
Webbink, R. F. 1984, ApJ, 277, 355
Welty, D. E., Ritchey, A. M., Dahlstrom, J. A., & York, D. G. 2014, arXiv:1404.2639
Welty, D. E., Xue, R., & Wong, T. 2012, ApJ, 745, 173
Whelan, J., & Iben, I., Jr. 1973, ApJ, 186, 1007
Wood-Vasey, W. M., & Sokoloski, J. L. 2006, ApJL, 645, L53
Yaron, O., Prialnik, D., Shara, M. M., & Kovetz, A. 2005, ApJ, 623, 398
Yoon, S.-C., & Langer, N. 2003, A&A, 412, L53
Yoon, S.-C., & Langer, N. 2005, A&A, 435, 967
Zheng, W., Shivvers, I., Filippenko, A. V., et al. 2014, ApJL, 783, L24